Generation of high-fidelity quantum control methods for multilevel systems

J. Randall,[1,2] A. M. Lawrence,[1,2] S. C. Webster,[1] S. Weidt,[1] N. V. Vitanov,[3] and W. K. Hensinger[1,*]

[1]*Department of Physics and Astronomy, University of Sussex, Brighton, BN1 9QH, United Kingdom*

[2]*QOLS, Blackett Laboratory, Imperial College London, London, SW7 2BW, United Kingdom*

[3]*Department of Physics, St. Kliment Ohridski University of Sofia, 5 James Bourchier Blvd, 1164 Sofia, Bulgaria*

(Received 7 February 2018; published 8 October 2018)

In recent decades there has been a rapid development of methods to experimentally control individual quantum systems. A broad range of quantum control methods has been developed for two-level systems; however, the complexity of multilevel quantum systems make the development of analogous control methods extremely challenging. Here we exploit the equivalence between multilevel systems with SU(2) symmetry and spin-1/2 systems to develop a technique for generating new robust, high-fidelity, multilevel control methods. As a demonstration of this technique, we develop adiabatic and composite multilevel quantum control methods and experimentally realize these methods using a $^{171}Yb^{+}$ ion system. We measure the average infidelity of the process in both cases to be around 10^{-4}, demonstrating that this technique can be used to develop high-fidelity multilevel quantum control methods and can, for example, be applied to a wide range of quantum computing protocols, including implementations below the fault-tolerant threshold in trapped ions.

DOI: 10.1103/PhysRevA.98.043414

I. INTRODUCTION

Quantum control methods are essential in many areas of experimental quantum physics, including trapped atoms, ions and molecules, and solid state systems [1–3]. Although the focus is often on two-level systems, in nearly all experimental realizations a larger number of states need to be taken into consideration, for example, to prepare a qubit in a two-level subspace of the system or to read out the state at the end of an experiment. In addition, the unique features of multilevel systems have led to new fields of research, including electromagnetically induced transparency [4] and single-photon generation [5]. Multilevel systems are also widely used in quantum computing, with applications such as the preparation and detection of dressed-state qubits [6,7]. A variety of multilevel methods including stimulated Raman adiabatic passage (STIRAP) [8], multistate extensions of Stark-chirped rapid adiabatic passage (SCRAP) [9], and other adiabatic methods involving chirped laser fields [10–12] have been developed, in addition to numerical algorithms for optimized quantum control [13]. However, the development of new control methods for multilevel systems (especially for high-fidelity operations) is challenging and often inhibited by the mathematical complexity of such higher-dimensional Hilbert spaces. Previous investigations into multilevel dynamics have studied coherent excitation of multilevel systems under the action of SU(2) Hamiltonians [14–18]. They showed that for a Hamiltonian with this symmetry there exists an equivalent Hamiltonian acting on a two-level system, and the dynamics of this two-level Hamiltonian can then be used to find solutions for the dynamics of the higher-dimensional system.

Here we apply this insight to find states in a two-level system that are equivalent to the states we wish to transform between in the multilevel system. This is key for practical quantum control methods where it is often necessary to transfer population between two particular states with high fidelity [1]. If such states exist, any method to move between them can be transformed into the multilevel case. Thus, we can transform robust, high-fidelity two-level methods into multilevel methods which also possess these desirable properties. We experimentally implement two control methods for trapped ions generated using the technique, demonstrating their high-fidelity and robustness.

The paper is organized as follows. In Sec. II we introduce the Majorana decomposition and detail how to design multilevel control methods using equivalent two-level methods. In Sec. III we introduce a three-level example system in $^{171}Yb^{+}$ and discuss the mapping to a two-level system for this specific case. In Secs. IV and V we demonstrate adiabatic and composite control methods based on the Majorana decomposition in our trapped ion system. Finally, in Sec. VI we present a measurement of the fidelity of the two control methods.

II. MAJORANA DECOMPOSITION

The Majorana decomposition was originally devised as a way of simplifying the dynamics of a spin-j system in an inhomogeneous magnetic field, by reducing the dynamics to that of an effective two-level system [14,15,19,20]. Consider a Hamiltonian that takes the same form as a spin in a magnetic field, $H_j = \mathbf{\Lambda}(t)\cdot\mathbf{J}$, where $\mathbf{J} = J_x\hat{\mathbf{x}} + J_y\hat{\mathbf{y}} + J_z\hat{\mathbf{z}}$, J_i being the angular momentum operators of a spin-j particle, and $\mathbf{\Lambda}(t)$ is a three-component vector specifying the control fields that we apply to our system. Such a system can be said to have SU(2) symmetry [17]. Majorana showed that the dynamics of such a system can be mapped exactly onto the dynamics of

*w.k.hensinger@sussex.ac.uk

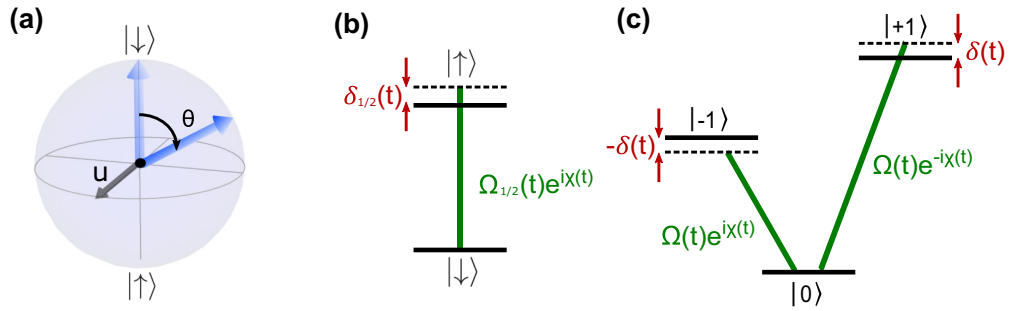

FIG. 1. Use of an effective two-level system to generate three-level control methods. (a) We wish to implement a control method which transforms an initial state $|\psi_{1/2}\rangle_{\rm i}$ on the effective two-level Bloch sphere (which here we take to be $|\downarrow\rangle$) into a final state $|\psi_{1/2}\rangle_{\rm f} = e^{-i\theta\hat{\mathbf{u}}\cdot\mathbf{S}}|\psi_{1/2}\rangle_{\rm i}$, where $\hat{\mathbf{u}}$ is the axis of rotation and θ is the angle (equivalent to $|\psi_j\rangle_{\rm f} = e^{-i\theta\hat{\mathbf{u}}\cdot\mathbf{J}}|\psi_j\rangle_{\rm i}$ in the real multilevel system). (b) In the effective two-level system, most control methods are implemented by applying a single control field of Rabi frequency $\Omega_{1/2}(t)$, instantaneous detuning $\delta_{1/2}(t)$, and phase $\chi(t)$. (c) By inverting the Majorana decomposition, we derive the control fields that we must apply to our real physical system, namely, two fields of equal Rabi frequency $\Omega(t)$ and equal and opposite detunings and phases $\pm\delta(t)$ and $\pm\chi(t)$, respectively.

a spin-1/2 particle, acted upon by the Hamiltonian $H_{1/2} = \mathbf{\Lambda}(t)\cdot\mathbf{S}$, $\mathbf{S}$ being the spin-1/2 angular momentum operator. This decomposition has been used to develop analytical solutions for the dynamics of a multilevel system [16,17]. Here we apply these ideas to generate high-fidelity multilevel quantum control methods. First, we use the Majorana decomposition to transform a multilevel problem into its much simpler two-level equivalent, for which a multitude of control methods are readily available. By then inverting the Majorana decomposition, we obtain the control fields for a new equivalent multilevel method.

In order to describe this technique, we introduce the following mathematical framework, which expresses each step of the process in simple, geometrical terms. First, consider an initial and final state in a multilevel system which we require to be related by a rotation $|\psi_j\rangle_{\rm f} = e^{-i\theta\hat{\mathbf{u}}\cdot\mathbf{J}}|\psi_j\rangle_{\rm i}$, where $\hat{\mathbf{u}}$ and θ specify the axis and angle of rotation, respectively. The Majorana decomposition tells us that there will be an equivalent transformation in the spin-1/2 system: $|\psi_{1/2}\rangle_{\rm f} = e^{-i\theta\hat{\mathbf{u}}\cdot\mathbf{S}}|\psi_{1/2}\rangle_{\rm i}$ [Fig. 1(a)], where the choice of $|\psi_{1/2}\rangle_{\rm i}$ is arbitrary. At this point we can use any of the many robust two-level control methods to carry out the transformation $|\psi_{1/2}\rangle_{\rm i} \to |\psi_{1/2}\rangle_{\rm f}$. To transform this two-level method into the new multilevel control method we apply the inverse of the Majorana decomposition. Noting that any two-level Hamiltonian can be written in the form $H_{1/2} = \mathbf{\Lambda}(t)\cdot\mathbf{S}$, we obtain the multilevel method by producing a Hamiltonian H_j with the same control vector $\mathbf{\Lambda}(t)$. This will perform the required multilevel state transformation $|\psi_j\rangle_{\rm i} \to |\psi_j\rangle_{\rm f}$. The new multilevel method will share desirable properties with the original two-level method, such as robustness to certain parameter errors that also have SU(2) symmetry.

As an example, suppose that we want to transfer population between eigenstates of two different angular momentum operators in different directions. The initial and final states $|\psi_j\rangle_{\rm i}$ and $|\psi_j\rangle_{\rm f}$ are eigenstates of the projection angular momentum operators along the directions $\hat{\mathbf{r}}_i$ and $\hat{\mathbf{r}}_f$, respectively, with the same eigenvalue m_J. Any rotation that transforms $\hat{\mathbf{r}}_i$ to $\hat{\mathbf{r}}_f$ will suffice. The simplest rotation (smallest rotation angle) is given by $\theta = \sin^{-1}(|\mathbf{r}_i \times \mathbf{r}_f|)$, $\hat{\mathbf{u}} = \mathbf{r}_i \times \mathbf{r}_f/|\mathbf{r}_i \times \mathbf{r}_f|$. For example, consider the J_z and J_x eigenstates for the $j = 1$ three-level system. The J_z eigenstates are the basis states $|+1\rangle$, $|0\rangle$, and $|-1\rangle$, with eigenvalues +1, 0, and −1, respectively, while the three eigenstates of J_x are $|u\rangle = \frac{1}{2}|+1\rangle + \frac{1}{2}|-1\rangle + \frac{1}{\sqrt{2}}|0\rangle$, $|D\rangle = (|+1\rangle - |-1\rangle)/\sqrt{2}$, and $|d\rangle = \frac{1}{2}|+1\rangle + \frac{1}{2}|-1\rangle - \frac{1}{\sqrt{2}}|0\rangle$, again with eigenvalues of +1, 0, and −1. We can consider the effect of consecutive rotations of $\pi/2$ about the y axis, that is, applications of the rotation operator $e^{-i(\pi/2)J_y}$. If we start in the state $|0\rangle$, then ignoring global phases we get the following sequence of states:

$$|0\rangle \to |D\rangle \to |0\rangle \to |D\rangle \to |0\rangle, \tag{1}$$

where the ion is alternating between the $m = 0$ eigenstates of the two angular momentum operators J_z and J_x, since the $m_J = 0$ eigenstates of a projection operator and its inverse are equal. If instead we start in $|+1\rangle$ we get the sequence

$$|+1\rangle \to |u\rangle \to |-1\rangle \to |d\rangle \to |+1\rangle, \tag{2}$$

where the ion is moving between the ±1 eigenstates of the J_z and J_x operators. Any two-level control method that rotates by an angle $\pi/2$ about the y axis can therefore be used to transform between states in the three-level system linked in Eqs. (1) and (2).

The method described in this section is a general technique to derive robust quantum control methods for multilevel systems based on the Majorana decomposition. In the following sections we will describe a specific physical system of interest, a three-level system in the ground state of a single trapped ion, and demonstrate the application of this method to robustly perform a specific desired state transformation within this system.

III. THREE-LEVEL TRAPPED ION SYSTEM

To illustrate the technique described in Sec. II, we generate control methods for the coherent manipulation of a three-level V-system. We demonstrate these methods experimentally using a single trapped $^{171}Yb^+$ ion, where the three levels $|+1\rangle$, $|0\rangle$, and $|-1\rangle$ correspond to the states $|F = 1, m_F = +1\rangle$, $|F = 0\rangle$, and $|F = 1, m_F = -1\rangle$ of the $^2S_{1/2}$ ground-state hyperfine manifold, respectively. The ion is confined in a linear Paul trap, details of which are described in Refs. [21,22]. A

magnetic field of $B_0 = 8.8305(4)$ G is applied using permanent magnets inside the vacuum system and external current coils. The magnetic field splits the energies of the states making up the $F = 1$ manifold. The transitions from $|0\rangle$ to $|\pm 1\rangle$ are driven by two microwave fields generated using an RF arbitrary waveform generator, which creates a waveform with a bandwidth of ≈30 MHz centered around 100 MHz. Typically we set the Rabi frequencies Ω_1 and Ω_2 of these applied fields to be equal, so that the dark state $|D\rangle$ will be an eigenstate of the dressed Hamiltonian [Eq. (4)]. The waveform is then frequency mixed with a signal near 12.5 GHz, before being amplified to 2 W and sent to a microwave horn positioned near a viewport of the vacuum system, approximately 2 cm from the ion. The ion is prepared in $|0\rangle$ using optical pumping, and a fluorescence measurement distinguishes between $|0\rangle$ and $\{|-1\rangle, |0'\rangle, |+1\rangle\}$, where $|0'\rangle \equiv |F = 1, m_F = 0\rangle$ is an additional state in the $F = 1$ manifold that is not used. A maximum likelihood method is used to normalize the data against independently measured state detection errors (Appendix A).

We would like to transfer the system from $|0\rangle$ to the superposition state $|D\rangle \equiv (|+1\rangle - |-1\rangle)/\sqrt{2}$, which can be protected against decoherence caused by fluctuating magnetic fields by the application of a pair of dressing fields [6,7] and has been shown to be useful for quantum computation [6,7,23–26] and magnetometry [27]. Previous methods to transfer population between these states either are susceptible to errors from fluctuating magnetic fields [6,7] or require the use of the $|0'\rangle$ state, which would ideally be reserved to form a qubit along with $|D\rangle$ [23]. It would therefore be desirable to design a robust method to transfer between these states with low infidelity. The required population transfer corresponds to the unitary transformation $U_{j=1} = e^{-i(\pi/2)J_y}$, a rotation about the y axis by $\pi/2$. Due to the Majorana decomposition, this is equivalent to the transformation $|\downarrow\rangle \rightarrow \frac{1}{\sqrt{2}}(|\downarrow\rangle + |\uparrow\rangle)$ in a spin-1/2 system, as shown in Sec. II [Fig. 1(a)].

There are many ways to carry out this two-level process, such as a simple $\pi/2$ pulse, or more robust methods such as composite pulses and adiabatic passage. The vast majority of two-level methods that can be implemented use a single control field, with possibly time-varying amplitude, frequency, and phase [Fig. 1(b)]. Moving to an interaction picture rotating at the frequency of the field, and after making the rotating wave approximation, this corresponds to a Hamiltonian

$$H_{1/2} = \frac{\hbar}{2}\begin{pmatrix} -\delta_{1/2}(t) & \Omega_{1/2}(t)e^{i\chi(t)} \\ \Omega_{1/2}(t)e^{-i\chi(t)} & \delta_{1/2}(t) \end{pmatrix} \tag{3}$$

(with the states ordered $|\downarrow\rangle, |\uparrow\rangle$), which can be written as $H_{1/2} = \hbar\{\Omega_{1/2}(t)\cos[\chi(t)]S_x + \Omega_{1/2}(t)\sin[\chi(t)]S_y + \delta_{1/2}(t)S_z\}$, where $\Omega_{1/2}(t)$, $\delta_{1/2}(t)$, and $\chi(t)$ are the time-varying Rabi frequency, instantaneous detuning, and phase, respectively. Once the forms of $\Omega_{1/2}(t)$, $\delta_{1/2}(t)$, and $\chi(t)$ have been chosen to perform the required transformation $|\downarrow\rangle \rightarrow \frac{1}{\sqrt{2}}(|\downarrow\rangle + |\uparrow\rangle)$, we can invert the Majorana decomposition to determine what real-world control fields we must apply to our physical three-level system to move between the initial and final states $|0\rangle$ and $|D\rangle$. The resulting three-level Hamiltonian is obtained by replacing the Pauli matrices in $H_{1/2}$ above with the three-level spin matrices J_i: $H_{j=1} = \hbar\{\Omega_{1/2}(t)\cos[\chi(t)]J_x + \Omega_{1/2}(t)\sin[\chi(t)]J_y + \delta_{1/2}(t)J_z\}$. This Hamiltonian can be written as

$$H_{j=1} = \frac{\hbar}{2}\begin{pmatrix} -\delta(t) & \Omega(t)e^{i\chi(t)} & 0 \\ \Omega(t)e^{-i\chi(t)} & 0 & \Omega(t)e^{i\chi(t)} \\ 0 & \Omega(t)e^{-i\chi(t)} & \delta(t) \end{pmatrix} \tag{4}$$

(with the states ordered $|-1\rangle, |0\rangle, |+1\rangle$), which corresponds to a pair of control fields, each of Rabi frequency $\Omega(t) = \sqrt{2}\Omega_{1/2}(t)$, with opposite phases $\pm\chi(t)$ and opposite detunings $\pm\delta(t) = \pm 2\delta_{1/2}(t)$ [Fig. 1(c)].

Now that we have derived a transformation between the effective two-level system and our physical three-level system, we can design new control methods to achieve the desired mapping based on existing two-level control methods. Quantum control methods for two-level systems are often designed to protect against errors caused by fluctuating parameters, such as detuning and Rabi frequency. These errors in a two-level system will also have equivalents in the multilevel case, and any protection offered will carry over. In the $^{171}Yb^+$ system used here, two main sources of error are caused by magnetic field noise and common mode Rabi frequency noise, the effects of which both have SU(2) symmetry and can therefore be countered by the appropriate choice of two-level control method. In the following sections, we design and demonstrate two such methods.

IV. ADIABATIC CONTROL METHOD

The first method is an adiabatic method following on from the work of Hioe [16], which is the three-level equivalent of the well-known two-level process of rapid adiabatic passage described by the Landau-Zener-Stuckelberg-Majorana model [28,29]. Here population is transferred between two states by adiabatically moving their energies to an avoided crossing. If the field is adiabatically varied from the regime where $\Omega_{1/2}/\delta_{1/2} = 0$, to $\Omega_{1/2}/\delta_{1/2} = \infty$ with $\chi = 0$ by turning the field on slowly while chirping the frequency, the population will be transferred from the initial eigenstate $|\downarrow\rangle$ to $(|\downarrow\rangle + |\uparrow\rangle)/\sqrt{2}$ [see Figs. 2(a) and 2(b)]. If we translate this into the three-level picture, we obtain a Hamiltonian of the form shown in Eq. (4). This describes an adiabatic process involving chirped pulses and amplitude shaping which transfers population from $|0\rangle$ to $|D\rangle$, similar to the analytical solution derived by Hioe [16].

A Blackman function [30] is used to define the form of the time-varying detuning $\delta(t)$. This pulse shape was chosen because in numerical simulations it produced the lowest infidelity due to nonadiabaticities. For a Blackman chirp profile starting at δ_0 and finishing at zero detuning, the required "instantaneous" detuning is

$$\delta(t) = \frac{\delta_0}{50}\left[21 + 25\cos\left(\frac{\pi t}{t_\delta}\right) + 4\cos\left(\frac{2\pi t}{t_\delta}\right)\right], \tag{5}$$

where t_δ is the detuning chirp time [Fig. 2(d)]. Due to the choice of interaction picture chosen to derive Eqs. (3) and (4), where the interaction frame is rotating at the time-dependent frequency of the field, this is the detuning used in these equations. In the laboratory frame, the required frequency of the physical field is given by $\omega_0 + \Delta(t)$, where ω_0 is the resonant frequency and $\Delta(t)$ is the detuning. However, $\Delta(t)$

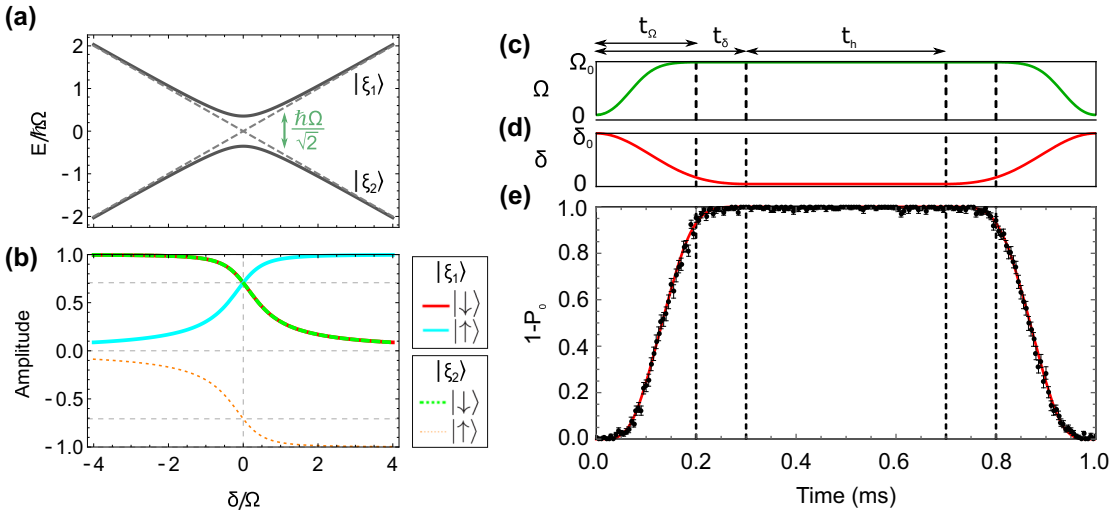

FIG. 2. Adiabatic transfer to the dark state of a dressed three-level system. (a) Energy eigenvalues and (b) eigenstates $\{|\xi_1\rangle, |\xi_2\rangle\}$ of $H_{1/2}$ as a function of δ/Ω for $\chi = 0$. (b) Analytically calculated amplitudes of these eigenstates, all of which can be defined as real numbers in this case. An avoided crossing is present at $\delta/\Omega = 0$, at which point the eigenstates are the dressed states $(|\downarrow\rangle \pm |\uparrow\rangle)/\sqrt{2}$, which are separated in energy by $\hbar\Omega/\sqrt{2}$. Therefore, by adiabatically varying the detuning and Rabi frequency, the population can be coherently transferred from $\{|\downarrow\rangle, |\uparrow\rangle\}$ to $(|\downarrow\rangle \pm |\uparrow\rangle)/\sqrt{2}$. (c–e) Demonstrating the method using a single $^{171}Yb^+$ ion. In the three-level system, the adiabatic procedure will transfer population from $|0\rangle$ to the dark state $|D\rangle = (|+1\rangle - |-1\rangle)/\sqrt{2}$. (c, d) The temporal profiles for the Rabi frequency Ω (solid green line in c) and the instantaneous detuning δ (solid red line in d), where the relevant parameters are given in the text. (e) Measured probability for the ion to be in the $^{171}Yb^+$ $F = 1$ state given by $P(F = 1) = 1 - P_0$ as a function of time. Each point is the average of 300 repetitions. The theoretical probability for the ion to be in $F = 1$ as a function of time (solid red line) is obtained from a numerical simulation of the system with no free parameters, which can be seen to agree well with the measured data.

is not equal to this instantaneous detuning of the field. The instantaneous frequency of a sinusoidal function at any given time is given by the time derivative of its overall phase, which in our case is equal to $\delta(t) = d(\Delta(t)t)/dt$ for $\chi(t) = 0$. The required profile for $\Delta(t)$ is therefore given by

$$\Delta(t) = \frac{1}{t}\int_0^t \delta(\tau)\,d\tau = \frac{\delta_0}{50t}\left\{21t + \frac{t_\delta}{\pi}\left[25\sin\left(\frac{\pi t}{t_\delta}\right) + 2\sin\left(\frac{2\pi t}{t_\delta}\right)\right]\right\}. \quad (6)$$

The amplitude of the driving fields are also changed during the first part of the detuning chirp. We again use a Blackman function, giving a Rabi frequency profile

$$\Omega(t) = \frac{\Omega_0}{50}\left[29 - 25\cos\left(\frac{\pi t}{t_\Omega}\right) - 4\cos\left(\frac{2\pi t}{t_\Omega}\right)\right], \quad (7)$$

where t_Ω is the amplitude ramp time [Fig. 2(c)]. The Rabi frequency is then kept constant at Ω_0 until the detuning chirp is complete.

We implement this procedure experimentally in our $^{171}Yb^+$ ion system. Figure 2(e) shows the probability of measuring the system in the $^{171}Yb^+$ $F = 1$ level $(1 - P_0)$ as a function of time during the adiabatic procedure. First, the transformation $|0\rangle \rightarrow |D\rangle$ is performed. Next, the system is left in the state $|D\rangle$, which is protected by the control fields, for a "hold" time $t_h = 400\,\mu s$. Finally, the inverse transformation $|D\rangle \rightarrow |0\rangle$ is performed by reversing the amplitude-shaping and chirped frequency profiles of the forward process. The optimal parameters for the Blackman profiles were found by simulations to be $\Omega_0/2\pi = 40\,kHz$, $\delta_0/2\pi = 60\,kHz$, $t_\Omega = 200\,\mu s$, and $t_\delta = 300\,\mu s$. Compression in the microwave amplifiers slightly alters the amplitude envelope of the applied microwave radiation compared with that generated by the arbitrary waveform generator. This effect, which has been included in the numerical simulation, has a negligible impact on the simulated fidelity. Plots of $\Omega(t)$ and $\delta(t)$ in Figs. 2(c) and 2(d) include these effects of compression.

V. COMPOSITE CONTROL METHOD

We have shown that our technique can be used to develop a three-level adiabatic method similar to the two-level method of rapid adiabatic passage. As a further demonstration of our technique to develop multilevel control methods, we implement a resonant control method to transfer population from $|0\rangle$ to $|D\rangle$. We do this by creating a three-level composite pulse sequence. A widely used example of a two-level composite pulse sequence is the BB_1 pulse sequence by Wimperis [31], which consists of four resonant Rabi pulses and can protect against pulse area errors. The four pulses of the BB_1 sequence carry out four consecutive rotations of the type $R(\theta_R, \phi_R)$, each with a particular choice of rotation angle θ_R and phase ϕ_R (corresponding to a rotation axis $\hat{\mathbf{u}} = \cos\phi_R\hat{\mathbf{x}} + \sin\phi_R\hat{\mathbf{y}}$). For a rotation from $\theta = \phi = 0$ to $\theta = \pi/2$, $\phi = 0$, it consists of four pulses and is given by $U(BB_1) = R(\pi/2, \pi/2) \cdot R(\pi, 3.267) \cdot R(2\pi, 0.376) \cdot R(\pi, 3.267)$, where $R(\theta_R, \phi_R)$ is a rotation on the Bloch sphere by polar angles θ_R and ϕ_R [see Fig. 3(a)].

Using our technique, we can produce an analogous control method for three-level systems which can robustly transfer

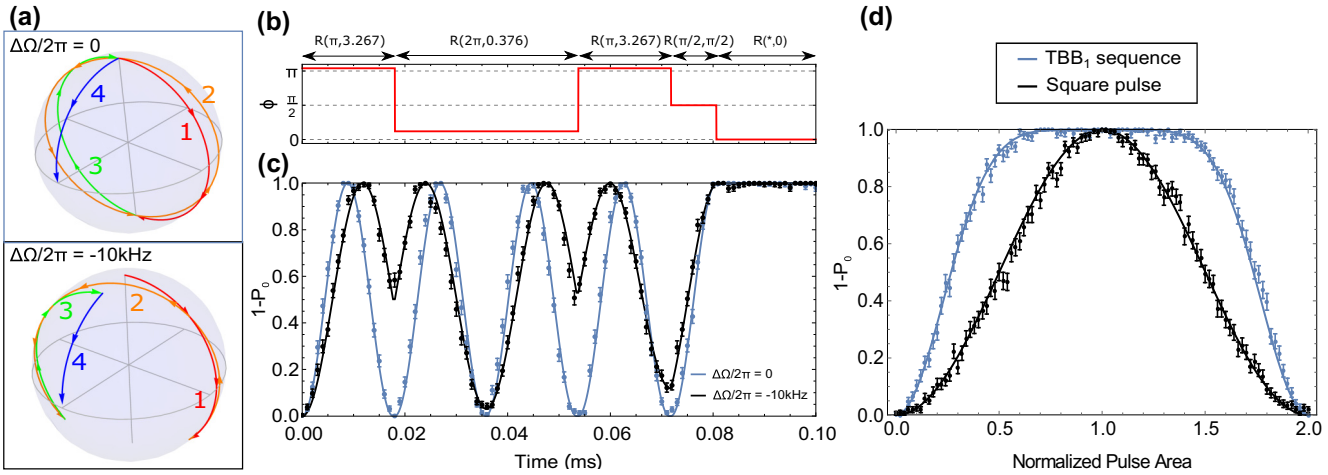

FIG. 3. Robust population transfer to the dark state using the TBB_1 composite pulse sequence. (a) The TBB_1 composite pulse sequence represented on the effective two-level Bloch sphere. The sequence consists of four resonant pulses with varying pulse area and phase which can be written as a sequence of rotations on the Bloch sphere of the form $R(\theta_R, \phi_R)$. Each of these rotations is represented as a colored line on the Bloch sphere, in the order red, orange, green, blue (numbered to show ordering). Above is the trajectory in the case of zero Rabi frequency error and below for the $\Delta\Omega = -2\pi \times 10\,\text{kHz}$ case. We implement both of these cases experimentally to demostrate the robustness of the method to pulse area errors. (b) The phase χ as a function of time implementing the TBB_1 pulse sequence for a fixed Rabi frequency $\Omega_0/2\pi = 40\,\text{kHz}$. An extra phase change of $-\pi/2$ at the end ensures the population remains in $|D\rangle$ after the procedure. Therefore the total pulse sequence is $R(*, 0) \cdot R(\pi/2, \pi/2) \cdot R(\pi, 3.267) \cdot R(2\pi, 0.376) \cdot R(\pi, 3.267)$. (c) The measured population in $F = 1$ as a function of time with $\Delta\Omega = 0$ (a, upper sphere; c, light blue line or light gray when printed in grayscale) and for a Rabi frequency error of $\Delta\Omega = -2\pi \times 10\,\text{kHz}$ (a, lower sphere; c, black line), showing that the sequence is robust to such errors. (d) Measured population in $F = 1$ as a function of pulse area for a square $\pi/2$ pulse (black) and the TBB_1 pulse sequence (light blue; light gray when printed in grayscale), demonstrating that the TBB_1 sequence maintains the robustness to pulse area error of the original two-level BB_1 sequence. The pulse area is normalized such that the nominal pulse area for a $\pi/2$ rotation is 1. The solid lines in panels (c) and (d) correspond to numerical simulations of the sequence with no free parameters.

population from $|0\rangle$ to $|D\rangle$ (which we call the TBB_1 sequence). This method consists of a sequence of simultaneous microwave pulses on the $|0\rangle$ to $|\pm 1\rangle$ transitions, with parameters set such that $\Omega_0 t/\sqrt{2} = \theta_R$, $\chi = \phi_R$, and $\delta = 0$. Therefore the three-level TBB_1 sequence consists of four pulses of length 17.7, 35.4, 17.7, and 8.8 μs and phases ± 1.63, ± 0.19, ± 1.63, and ± 0.79 on the $|0\rangle$ to $|\pm 1\rangle$ transitions. Thus a rotation from $|0\rangle$ to $|D\rangle$ (which again is $|\downarrow\rangle$ to $(|\downarrow\rangle + |\uparrow\rangle)/\sqrt{2}$ in the effective two-level system) is implemented. In order to protect the $|D\rangle$ state after the sequence, the control fields are simply left on, with the relative phase χ set to 0. Figure 3(c) shows the population in $F = 1$ as a function of time during the TBB_1 pulse sequence for two cases. In one case the Rabi frequency is set to the correct value such that $\Delta\Omega = \Omega - \Omega_0 = 0$, while in the second case the Rabi frequency is deliberately misset by $\Delta\Omega = -2\pi \times 10\,\text{kHz}$, which corresponds to a 25% error in the applied microwave amplitude. It can be seen that in both cases the final population is almost entirely transferred to the $F = 1$ manifold, demonstrating the robustness of the composite sequence to substantial errors in the pulse area. The TBB_1 sequence is completed in a time of 80 μs compared to 300 μs for the adiabatic method, but both methods could be sped up by increasing the applied microwave power (i.e., raising the Rabi frequency). Figure 3(d) shows the population in $F = 1$ as a function of normalized pulse area for a single pulse nominally driving a rotation $R(\pi/2, \pi/2)$ in the effective two-level system, as well as when the TBB_1 pulse sequence is applied. The improvement in robustness of the TBB_1 sequence compared to the single pulse can clearly be seen, demonstrating that composite quantum control techniques developed for two-level systems give the same advantages in the three-level case.

VI. FIDELITY MEASUREMENTS

Although the data presented in Figs. 2 and 3 show a good agreement with theory, the fluorescence measurement scheme used can determine only the values of the quantities P_0 and $P_{+1} + P_{-1} + P_{0'} = 1 - P_0$, where $P_j = \langle j|\rho|j\rangle$ and ρ is the measured state. This is not sufficient to calculate the fidelity with which the state $|D\rangle$ is prepared. Therefore a more complex method is required to fully characterize the state fidelity. The fidelity of $|D\rangle$ is given by

$$\mathcal{F}_D \equiv \langle D|\rho|D\rangle = \frac{1}{2}(P_{+1} + P_{-1}) + |\rho_\pm| \cos(\phi_\pm), \qquad (8)$$

where we have written the off-diagonal matrix elements in polar form as $\rho_{+1,-1} \equiv |\rho_\pm| e^{i\phi_\pm} = \rho^*_{-1,+1}$. To measure this fidelity, an additional resonant pulse on the $|0\rangle$ to $|\pm 1\rangle$ transitions [Eq. (4); Fig. 4(a)] is applied for a time $t = \pi/2\Omega_{1/2}$ (we apply this pulse simply by leaving the microwave fields on after the sequence and stepping the phase by χ). If the phase χ is varied, the population in $|0\rangle$ is given by

$$P_0(\chi) = \tfrac{1}{2}(P_{+1} + P_{-1}) + |\rho_\pm| \cos(2\chi + \phi_\pm), \qquad (9)$$

where P_{+1}, P_{-1}, and $\rho_\pm$ are density matrix elements of the state before the additional pulse is applied. Comparing with Eq. (8), it can be seen that the offset, amplitude, and phase offset of the resulting sinusoidal curve can be used to calculate $\mathcal{F}_D$. Figure 4(b) shows the result of such an experiment after

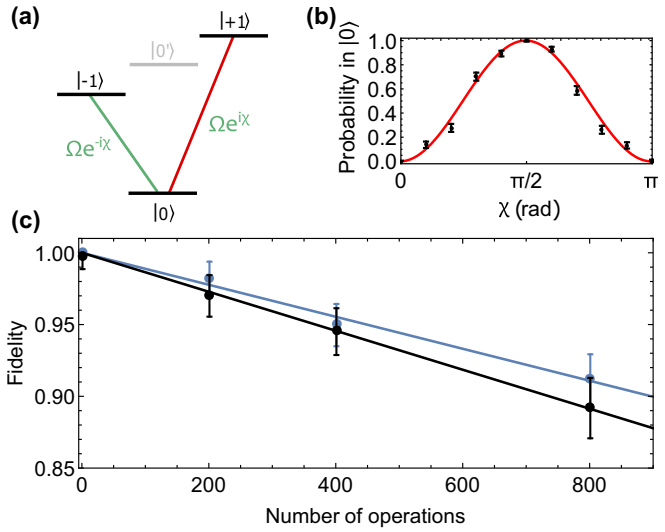

FIG. 4. Measuring the fidelity. (a) The fidelity with which we produce the $|D\rangle$ state can be obtained by applying two fields resonant with the $|0\rangle \leftrightarrow |+1\rangle$ and $|0\rangle \leftrightarrow |-1\rangle$ transitions with equal Rabi frequency Ω, and varying the phase χ of the two fields in equal and opposite directions. (b) The measured population in $|0\rangle$ as a function of χ after a single adiabatic operation (black points), which can be fitted to the function $A_0 + A\cos(2\chi + \phi_0)$ (solid red curve) to extract the mapping fidelity using a maximum likelihood fitting method (Appendix A). Each point is the average of 200 repetitions. (c) The fidelity as a function of the number of applications of the adiabatic method (black) and resonant TBB_1 sequence (light blue; light gray when printed in grayscale). For the adiabatic method, the population transfer back to $|0\rangle$ begins immediately after it reaches $|D\rangle$ ($t_h = 0$). A linear least-squares fit to the data gives an average infidelity per operation of $1.4(4) \times 10^{-4}$ for the adiabatic method and $1.1(4) \times 10^{-4}$ for the composite pulse sequence.

a single adiabatic transfer operation from $|0\rangle$ to $|D\rangle$. The data is fitted using maximum likelihood estimation (Appendix A) with the fit function $A_0 + A\cos(2\chi + \phi_0)$, giving fit parameters $A_0 = 0.500(4)$, $A = 0.500(3)$, and $\phi_0 = 3.16(3)$. This gives a map infidelity of $\mathcal{F}_D = 1.000(7)$. To obtain a more accurate infidelity estimate we must average over a large number of operations. The fidelity can be measured after N operations for multiple values of N, from which the average infidelity $1 - \overline{\mathcal{F}}_D$ can be calculated. This method is used to calculate the average fidelities of both the adiabatic and composite quantum control procedures. We measure an average infidelity per operation of $1.4(4) \times 10^{-4}$ for the adiabatic method and $1.1(4) \times 10^{-4}$ for the composite pulse sequence [32].

The experimentally achieved fidelity of the adiabatic control method is determined by two factors: the first is infidelities introduced during the operation due to nonadiabaticity of the frequency and amplitude modulation and decoherence, and the second is the precision with which the parameters of the applied radiation fields can be set, as they determine the final state obtained, which we call $|\psi_{\mathrm{dr}}\rangle$. By repeatedly applying the forward and reverse adiabatic operations we can determine the first of these infidelities, because to first order they will be amplified by the number of repeats to a measurable level. We do not attempt to measure the second infidelity $1 - |\langle D|\psi_{\mathrm{dr}}|^2$ as we do not have a process to amplify this infidelity, and any direct measurement is subject to the same inaccuracies in parameter setting. Instead we can estimate the size of this infidelity given the precision we can set the parameters of the radiation fields. The parameters in question are how equal the Rabi frequencies of the two fields can be set, and the accuracy to which the detuning of the two radiation fields can be set to zero. We determined that we set the fractional accuracy of the Rabi frequencies $|\Omega_1 - \Omega_2|/(\Omega_1 + \Omega_2) < 0.0015$ and that each of the detunings is set such that $|\delta| < 3\,\mathrm{Hz}$. From simulations, this leads to an infidelity of preparing $|D\rangle$ of $<10^{-4}$. We also note that for many applications, such as the use of the $|D\rangle$ and $|0'\rangle$ states as a qubit, this second infidelity has only a small effect on the overall fidelity of qubit operations. This "dressed-state qubit" is used because the coherence of the qubit is protected against magnetic field fluctuations [6,7]. In the event of a slight Rabi frequency mismatch or detuning error, the dressed state produced will not be exactly $|D\rangle$, but this state and $|0'\rangle$ will still form a valid qubit which will still be insensitive to magnetic field noise to first order.

The measured infidelities are consistent with the lifetime of the $|D\rangle$ state, which was measured in a separate experiment to be 2.6(4) s. The lifetime of $|D\rangle$ is limited by ambient magnetic field noise with frequency close to the dressed-state energy splitting. Since ambient noise generally scales as $\sim 1/f$, increasing the dressing field Rabi frequency is expected to improve this result [7]. We have also verified that the coherence of a $\{|0'\rangle, |D\rangle\}$ qubit is preserved throughout such an adiabatic transfer (Appendix C).

VII. CONCLUSION

In this article, we have used the Majorana decomposition to develop a technique for generating coherent control methods to transform between two desired multilevel states, based on existing two-level methods. This allows insights gained into robust control of two-level systems to be harnessed and applied to multilevel quantum control in a rigorous and analytical way. We have applied this technique to two well-known composite pulse and adiabatic methods to create three-level methods and have implemented these experimentally with high fidelity. These methods may be particularly important for the implementation of scalable quantum computing [33]. The technique we use to generate quantum control methods is general and can be applied to different quantum systems with arbitrary numbers of levels (Appendix D). Furthermore, we have shown that the control methods generated can be robust and applied with high fidelity. Therefore we believe this approach shows great promise for high-fidelity quantum control across a broad range of physical systems.

ACKNOWLEDGMENTS

We would like to thank Bruce Shore for providing us with very useful insights on the theory of multilevel quantum control. This work is supported by the UK Engineering and Physical Sciences Research Council [(EP/G007276/1), the UK Quantum Technology hub for Networked Quantum Information Technologies (EP/M013243/1), and the

UK Quantum Technology hub for Sensors and Metrology (EP/M013294/1)], the European Commission's Seventh Framework Programme (FP7/2007-2013) under grant agreement no. 270843 Integrated Quantum Information Technology, the Army Research Laboratory under cooperative agreement no. W911NF-12-2-0072, the US Army Research Office under contract no. W911NF-14-2-0106, and the University of Sussex. N.V.V. acknowledges support by the Bulgarian Science Fund Grant No. DN 18/14.

APPENDIX A: STATISTICAL METHODS

To normalize the data against state detection errors, before each experiment a histogram of fluorescence measurements is taken after preparing the ion in both the $|0\rangle$ and $|0'\rangle$ states, corresponding to dark and bright expected results, respectively. Using a threshold of two photons, the detection fidelity is typically measured to be around 97%. A linear map can then be extracted from the measured errors, which gives the probability to measure a bright event as $p_b(p) = P(b|1)p + P(b|0)(1-p)$, where p is the probability that the population was in the $F = 1$ manifold and $P(b|1)$ and $P(b|0)$ are the probabilities for a bright measurement given that the ion was in the $F = 1$ and $F = 0$ manifolds, respectively. The data are scaled using a maximum likelihood method based on a binomial distribution. This maximizes the log-likelihood function for a beta probability density function, given by

$$f_B = \sum_{i=1}^{N} \log\left\{\frac{(n+1)n!p_b(p_i)^{k_i}[1-p_b(p_i)]^{n-k_i}}{k_i!(n-k_i)!}\right\}, \quad \text{(A1)}$$

where n is the number of repetitions per data point, N is the number of data points, and k_i is the number of bright events for the ith data point. For individual data points, $N = 1$, and therefore p_1 is found by maximizing f_B for k_1. To fit the fidelity measurements shown in Fig. 4, the probabilities are replaced by a fit function $p_i = A_0 + A\cos(2\chi_i + \phi_0)$. In this case, f_B is maximized over all N data points for different χ_i, and the best fit parameters for A_0, A, and ϕ_0 are extracted. The state fidelity is then given by $\mathcal{F}_D = A_0 - A\cos(\phi_0)$, which is plotted as a function of the number of maps in Fig. 4(c). A linear least-squares fit is then applied with the fit function $1 - x\epsilon_m$, where x is the number of maps and $\epsilon_m = 1 - \overline{\mathcal{F}}_D$ is the average infidelity per map.

APPENDIX B: SPIN-J REPRESENTATION OF ARBITRARY SPIN-1/2 UNITARIES

As well as the mapping between initial and final states, it is also useful to derive a theoretical solution for the intermediate state of the multilevel system during application of the control fields. One option is to consider at arbitrary times during the transformation the equivalent rotation matrix in the multilevel system. However, rather than doing this explicitly, the unitary operation in the multilevel system can be directly calculated from the unitary operation in the two-level system. The spin-1/2 state $|\Psi_{1/2}\rangle = a|\downarrow\rangle + b|\uparrow\rangle$ is obtained by applying the general unitary

$$U^{\frac{1}{2}} = \begin{pmatrix} a & -b^* \\ b & a^* \end{pmatrix} \quad \text{(B1)}$$

to the initial state $|\downarrow\rangle$. From this unitary, the unitary in the multilevel system can be calculated directly. For the general spin-j system, the matrix elements of U_j are given by [15,34]

$$U^j_{rs} = \sum_{q=q_{\min}}^{q_{\max}} \sqrt{C^{r-1}_q C^{s-1}_q C^{2j+1-r}_{s-1-q} C^{2j+1-s}_{r-1-q}} \times a^{2j+2-r-s+q}(a^*)^q b^{s-1+q}(-b^*)^{r-1+q}, \quad \text{(B2)}$$

where $q_{\min} = \max[0, r+s-2j]$ and $q_{\max} = \min[r-1, s-1]$ and $C^n_k = n!/[k!(n-k)!]$ is the binomial coefficient. For the $j = 1$ case, this results in the unitary transformation [16]

$$U^{j=1} = \begin{pmatrix} a^2 & -ab^*\sqrt{2} & b^{*2} \\ ab\sqrt{2} & |a|^2 - |b|^2 & -a^*b^*\sqrt{2} \\ b^2 & a^*b\sqrt{2} & a^{*2} \end{pmatrix}. \quad \text{(B3)}$$

APPENDIX C: DRESSED STATE QUBIT MAPPING

In the context of a scalable microwave-driven trapped ion quantum computing architecture [25,33], it is useful to map the state of a qubit stored in the $\{|0\rangle, |0'\rangle\}$ basis of an $^{171}Yb^+$ ion to the $\{|D\rangle, |0'\rangle\}$ basis. This can be done by implementing either the adiabatic or the resonant method to transfer any population in state $|0\rangle$ to $|D\rangle$. While we have verified that this population transfer process can be implemented with high fidelity, this does not necessarily indicate that the coherence of the qubit is maintained throughout the population transfer process. Therefore we carried out a Ramsey-type experiment to measure the coherence of the qubit before and after the mapping, in the case of the adiabatic transfer method.

In these Ramsey experiments, we start with a resonant $\pi/2$ pulse on the $|0\rangle$ to $|0'\rangle$ "clock" transition to put the ion in the state $(|0\rangle + |0'\rangle)/\sqrt{2}$. Then we carry out $N/2$ adiabatic processes to map population back and forth between $|0\rangle$ and $|D\rangle$, followed by a spin echo π pulse on the clock transition, followed by $N/2$ adiabatic transfers. We then apply a final $\pi/2$ analysis pulse with varying phase and carry out a fluorescence measurement. As the phase is varied, we will see fringes in the measured population, just as in a standard Ramsey experiment. If there is any decoherence of the stored qubit, the amplitude of the fringes will decay. By fitting the population in $F = 1$ as a function of the phase of the final pulse, we can obtain the fidelity with which the qubit state is preserved. The decay of the fidelity with increasing N is then measured in a similar way to before. This allows us to extract the average infidelity of the qubit mapping process, which is found to be $1 - \overline{\mathcal{F}} = 1.8(4) \times 10^{-4}$.

APPENDIX D: APPLICATIONS TO OTHER D-LEVEL SYSTEMS

The technique described in this paper is general and can be applied to systems of arbitrary numbers of levels in a variety of quantum control applications. To illustrate this we provide two examples of potential applications in different quantum systems.

First, we refer to the work of Liu *et al.* [35], who proposed a method to transfer the state of one d-level superconducting qudit to another in circuit QED. They illustrate their method

in detail for the five-level case and show that it can be generalized to any number of levels. The method involves successively swapping over the population of different levels from one qudit to another via a cavity mode. By the end of step IV of their process (Fig. 2 of Ref. [35]) they have transferred the population of each individual state to the second qubit, but the states are in the wrong order. Therefore, in the final step of their process, Liu *et al.* apply a succession of pulses on different transitions within the qudit to rearrange the state populations so that they are in the exact reverse order compared to where they started. At this point the qudit transfer process is complete.

Here we show that, using our technique, a multilevel control method can instead be found to put the state populations back in their original order (not reversed) in a single step. Specifically, one must apply this four-level method to the top four levels of the second qudit (Fig. 2 of Ref. [35]) so as to reverse the order of their amplitudes. The required unitary matrix to carry out this operation is as follows:

$$U^{j=\frac{3}{2}} = \begin{pmatrix} 0 & 0 & 0 & 1 \\ 0 & 0 & 1 & 0 \\ 0 & 1 & 0 & 0 \\ 1 & 0 & 0 & 0 \end{pmatrix}, \tag{D1}$$

and we are looking for a quantum control method to implement this unitary operation. This unitary transformation is (up to a global phase which can be easily accounted for by changing the phases of the other pulses in the sequence) equal to $e^{-i\pi J_x}$, which is a rotation of exactly the form we need to derive multilevel quantum control method using our technique. The equivalent two-level rotation is simply $e^{-i\pi S_x}$, which can be achieved by a variety of quantum control methods: for example, a simple Rabi π-pulse or, if more robustness is required, more complex composite pulse or adiabatic schemes. The exact form of the control fields used to execute this transformation will depend on the exact control method used to implement the effective two-level rotation. In general, for a single control field applied to a two-level system, the two-level Hamiltonian of Eq. (3) must be transformed into a four-level Hamiltonian using the spin-3/2 matrices. Physically, this Hamiltonian, which represents the desired quantum control method, will correspond to three different control fields on the four-level system, of varying Rabi frequencies and detunings.

Liu *et al.* [35] discuss in their work how their method generalizes to d levels. Our four-level method also has a d-level equivalent which can reverse the populations of any number of states. One can verify this by noting that if you substitute $a = 0, b = i$ into Eq. (B2) one obtains

$$U^j_{rs} = i^{d+1}\delta_{d+1,r+s}, \tag{D2}$$

where $d = 2j + 1$ is the number of levels and δ_{ij} is the Kronecker delta. This is indeed a unitary operation, which reverses the order of the amplitudes for a d-level system.

Finally we consider the efficient Toffoli gate scheme discussed in Refs. [36,37]. Here the three-level unitary operation

$$X_a = \begin{pmatrix} 0 & 0 & 1 \\ 0 & 1 & 0 \\ 1 & 0 & 0 \end{pmatrix} \tag{D3}$$

is applied to a qutrit as part of the scheme. It is easy to verify that X_a is in fact equal to U^j_{rs} in Eq. (D3) in the case where $d = 3$ (up to an irrelevant global phase), showing that this control operation is also amenable to the techniques described in this paper.

[1] S. J. Glaser *et al.*, Training Schrödinger's cat: Quantum optimal control, Eur. Phys. J. D. **69**, 279 (2015).

[2] H. Mabuchi and K. Navin, Principles and applications of control in quantum systems, Intl. J. Robust Nonlinear Control **15**, 647 (2005).

[3] L. M. K. Vandersypen and I. L. Chuang, NMR techniques for quantum control and computation, Rev. Mod. Phys. **76**, 1037 (2004).

[4] M. Fleischhauer, A. Imamoglu, and J. P. Marangos, Electromagnetically induced transparency: Optics in coherent media, Rev. Mod. Phys. **77**, 633 (2005).

[5] A. Kuhn, M. Hennrich, and G. Rempe, Deterministic Single-Photon Source for Distributed Quantum Networking, Phys. Rev. Lett. **89**, 067901 (2002).

[6] N. Timoney *et al.*, Quantum gates and memory using microwave-dressed states, Nature (London) **476**, 185 (2011).

[7] S. C. Webster, S. Weidt, K. Lake, J. J. McLoughlin, and W. K. Hensinger, Simple Manipulation of a Microwave Dressed-State Ion Qubit, Phys. Rev. Lett. **111**, 140501 (2013).

[8] J. R. Kuklinski, U. Gaubatz, F. T. Hioe, and K. Bergmann, Adiabatic population transfer in a three-level system driven by delayed laser pulses, Phys. Rev. A **40**, 6741 (1989).

[9] A. A. Rangelov, N. V. Vitanov, L. P. Yatsenko, B. W. Shore, T. Halfmann, and K. Bergmann, Stark-shift-chirped rapid-adiabatic-passage technique among three states, Phys. Rev. A **72**, 053403 (2005).

[10] B. Broers, H. B. van Linden van den Heuvell, and L. D. Noordam, Efficient Population Transfer in a Three-Level Ladder System by Frequency-Swept Ultrashort Laser Pulses, Phys. Rev. Lett. **69**, 2062 (1992).

[11] J. S. Melinger, S. R. Gandhi, A. Hariharan, J. X. Tull, and W. S. Warren, Generation of Narrowband Inversion with Broadband Laser Pulses, Phys. Rev. Lett. **68**, 2000 (1992).

[12] N. V. Vitanov, T. Halfmann, B. W. Shore, and K. Bergmann, Laser-induced population transfer by adiabatic passage techniques, Annu. Rev. Phys. Chem. **52**, 763 (2001).

[13] N. Khaneja, T. Reiss, C. Kehlet, T. Schulte-Herbrüggen, and S. J. Glaser, Optimal control of coupled spin dynamics: Design of NMR pulse sequences by gradient ascent algorithms, J. Magn. Reson. **172**, 296 (2005).

[14] E. Majorana, Atomi orientati in campo magnetico variabile, Nuovo Cimento (1924–1942) **9**, 43 (1932).

[15] F. Bloch and I. I. Rabi, Atoms in variable magnetic fields, Rev. Mod. Phys. **17**, 237 (1945).

[16] F. T. Hioe, N-level quantum systems with SU(2) dynamic symmetry, J. Opt. Soc. Am. B **4**, 1327 (1987).
[17] R. J. Cook and B. W. Shore, Coherent dynamics of n-level atoms and molecules. III. An analytically soluble periodic case, Phys. Rev. A **20**, 539 (1979).
[18] G. T. Genov, B. T. Torosov, and N. V. Vitanov, Optimized control of multistate quantum systems by composite pulse sequences, Phys. Rev. A **84**, 063413 (2011).
[19] T. H. Bergeman, P. McNicholl, J. Kycia, H. Metcalf, and N. L. Balazs, Quantized motion of atoms in a quadrupole magnetostatic trap, J. Opt. Soc. Am. B **6**, 2249 (1989).
[20] A. Bauch and R. Schröder, Frequency shifts in a cesium atomic clock due to Majorana transitions, Ann. Phys. **505**, 421 (1993).
[21] J. J. McLoughlin, A. H. Nizamani, J. D. Siverns, R. C. Sterling, M. D. Hughes, B. Lekitsch, B. Stein, S. Weidt, and W. K. Hensinger, Versatile ytterbium ion trap experiment for operation of scalable ion-trap chips with motional heating and transition-frequency measurements, Phys. Rev. A **83**, 013406 (2011).
[22] K. Lake, S. Weidt, J. Randall, E. D. Standing, S. C. Webster, and W. K. Hensinger, Generation of spin-motion entanglement in a trapped ion using long-wavelength radiation, Phys. Rev. A **91**, 012319 (2015).
[23] J. Randall, S. Weidt, E. D. Standing, K. Lake, S. C. Webster, D. F. Murgia, T. Navickas, K. Roth, and W. K. Hensinger, Efficient preparation and detection of microwave dressed-state qubits and qutrits with trapped ions, Phys. Rev. A **91**, 012322 (2015).
[24] S. Weidt, J. Randall, S. C. Webster, E. D. Standing, A. Rodriguez, A. E. Webb, B. Lekitsch, and W. K. Hensinger, Ground-State Cooling of a Trapped Ion Using Long-Wavelength Radiation, Phys. Rev. Lett. **115**, 013002 (2015).
[25] S. Weidt, J. Randall, S. C. Webster, K. Lake, A. E. Webb, I. Cohen, T. Navickas, B. Lekitsch, A. Retzker, and W. K. Hensinger, Trapped-Ion Quantum Logic with Global Radiation Fields, Phys. Rev. Lett. **117**, 220501 (2016).
[26] A. Bermudez, F. Jelezko, M. B. Plenio, and A. Retzker, Electron-Mediated Nuclear-Spin Interactions Between Distant Nitrogen-Vacancy Centers, Phys. Rev. Lett. **107**, 150503 (2011).
[27] I. Baumgart, J. M. Cai, A. Retzker, M. B. Plenio, and C. Wunderlich, Ultrasensitive Magnetometer Using a Single Atom, Phys. Rev. Lett. **116**, 240801 (2016).
[28] L. Landau, On the theory of transfer of energy at collisions II, Phys. Z. Sowjetunion **2**, 46 (1932).
[29] C. Zener, Non-adiabatic crossing of energy levels, Proc. R. Soc. London A **137**, 696 (1932).
[30] R. B. Blackman and J. W. Tukey, Particular pairs of windows, in *The Measurement of Power Spectra, From the Point of View of Communications Engineering* (Dover, New York, 1959), pp. 98–99.
[31] S. Wimperis, Broadband, narrowband, and passband composite pulses for use in advanced NMR experiments, J. Magn. Reson., Ser. A **109**, 221 (1994).
[32] A recent study has suggested that the true infidelities may actually be somewhat lower than this, because infidelities due to coherent effects may be overestimated by this method [38]. However, as we believe our infidelities to be dominated by incoherent effects such as decoherence, this effect may not be significant.
[33] B. Lekitsch *et al.*, Blueprint for a microwave trapped ion quantum computer, Sci. Adv. **3**, e1601540 (2017).
[34] B. T. Torosov and N. V. Vitanov, Evolution of superpositions of quantum states through a level crossing, Phys. Rev. A **84**, 063411 (2011).
[35] T. Liu *et al.*, Transferring arbitrary d-dimensional quantum states of a superconducting transmon qudit in circuit QED, Sci. Rep. **7**, 7039 (2017).
[36] T. C. Ralph, K. Resch, and A. Gilchrist, Efficient Toffoli gates using qudits, Phys. Rev. A **75**, 022313 (2007).
[37] B. P. Lanyon *et al.*, Simplifying quantum logic using higher-dimensional Hilbert spaces, Nat. Phys. **5**, 134 (2008).
[38] N. V. Vitanov, Relations between the single-pass and double-pass transition probabilities in quantum systems with two and three states, Phys. Rev. A **97**, 053409 (2018).